Received: 19 February 2022 | Revised: 26 April 2022 | Accepted: 24 May 2022

DOI: 10.1002/mp.15785

RESEARCH ARTICLE

MEDICAL PHYSICS

Patient-derived heterogeneous breast phantoms for advanced dosimetry in mammography and tomosynthesis

Marco Caballo[1,†] | **Carolina Rabin**[2,†] | **Christian Fedon**[1,‡] | **Alejandro Rodríguez-Ruiz**[1,3] | **Oliver Diaz**[4] | **John M. Boone**[5] | **David R. Dance**[6] | **Ioannis Sechopoulos**[1,7,8]

[1]Department of Medical Imaging, Radboud University Medical Center, Nijmegen, The Netherlands

[2]Facultad de Ciencias, Instituto de Física, Universidad de la República, Montevideo, Uruguay

[3]Department of Image Guided Therapy Systems, Philips Healthcare, Eindhoven, The Netherlands

[4]Department of Mathematics and Computer Science, University of Barcelona, Barcelona, Spain

[5]Department of Radiology and Biomedical Engineering, University of California Davis Health, Sacramento, California, USA

[6]National Co-ordinating Centre for the Physics of Mammography (NCCPM), Royal Surrey County Hospital, Department of Physics, University of Surrey, Guildford, UK

[7]Dutch Expert Centre for Screening (LRCB), Nijmegen, The Netherlands

[8]Technical Medicine Centre, University of Twente, Enschede, The Netherlands

Correspondence
Ioannis Sechopoulos, Department of Medical Imaging, Radboud University Medical Center, PO Box 9101, 6500 HB Nijmegen, The Netherlands.
Email: Ioannis.Sechopoulos@radboudumc.nl

[†]Marco Caballo and Carolina Rabin contributed equally to this work as co-first authors.
[‡]Christian Fedon now at Nuclear Research and Consultancy Group (NRG), Westerduinweg 3, 1755 ZG Petten, The Netherlands.

Funding information
National Cancer Institute, National Institutes of Health, Grant/Award Number: R01CA181171; Susan G. Komen Foundation for the Cure, Grant/Award Number: IIR13262248

Abstract

Background: Understanding the magnitude and variability of the radiation dose absorbed by the breast fibroglandular tissue during mammography and digital breast tomosynthesis (DBT) is of paramount importance to assess risks versus benefits. Although homogeneous breast models have been proposed and used for decades for this purpose, they do not accurately reflect the actual heterogeneous distribution of the fibroglandular tissue in the breast, leading to biases in the estimation of dose from these modalities.

Purpose: To develop and validate a method to generate patient-derived, heterogeneous digital breast phantoms for breast dosimetry in mammography and DBT.

Methods: The proposed phantoms were developed starting from patient-based models of compressed breasts, generated for multiple thicknesses and representing the two standard views acquired in mammography and DBT, that is, cranio-caudal (CC) and medio-lateral-oblique (MLO). Internally, the breast phantoms were defined as consisting of an adipose/fibroglandular tissue mixture, with a nonspatially uniform relative concentration. The parenchyma distributions were obtained from a previously described model based on patient breast computed tomography data that underwent simulated compression. Following these distributions, phantoms with any glandular fraction (1%–100%) and breast thickness (12–125 mm) can be generated, for both views. The phantoms were validated, in terms of their accuracy for average normalized glandular dose (D_gN) estimation across samples of patient breasts, using 88 patient-specific phantoms involving actual patient distribution of the fibroglandular tissue in the

breast, and compared to that obtained using a homogeneous model similar to those currently used for breast dosimetry.
Results: The average D_gN estimated for the proposed phantoms was concordant with that absorbed by the patient-specific phantoms to within 5% (CC) and 4% (MLO). These D_gN estimates were over 30% lower than those estimated with the homogeneous models, which overestimated the average D_gN by 43% (CC), and 32% (MLO) compared to the patient-specific phantoms.
Conclusions: The developed phantoms can be used for dosimetry simulations to improve the accuracy of dose estimates in mammography and DBT.

KEYWORDS
breast density, breast dosimetry, digital breast tomosynthesis, digital phantoms, mammography

1 | INTRODUCTION

Understanding the magnitude and variability of the absorbed dose resulting from medical imaging modalities involving ionizing radiation is important when assessing risks versus benefits, especially for screening modalities. Given the widespread use of digital mammography and, in some areas of the world, digital breast tomosynthesis (DBT) for breast cancer screening, breast dosimetry has been a subject of extensive study. In the breast, the fibroglandular tissue is the most radiosensitive, and therefore the tissue at the highest risk of developing cancer. Hence, in breast imaging, the absorbed dose of primary concern is that deposited in the fibroglandular tissue.[1–6] A comprehensive overview of breast dosimetry and its history has been previously published.[7] The most basic current breast models for dosimetry assume that the breast consists of an outer layer of skin surrounding a homogeneous 50%–50% mixture of adipose and fibroglandular tissue. Variations of this model have been used for decades,[3–5] and numerous studies have been performed to investigate the dependence of the mean glandular dose with different breast thicknesses, sizes, and proportions of adipose/fibroglandular tissue mixtures (i.e., glandular fractions), both in mammography and DBT.[6–10]

With advancements in technology, especially with the development of fully three-dimensional (3D) dedicated breast computed tomography (breast CT),[11] a better characterization of the inner breast structure was made possible. This opened the door to an accurate quantification and localization of the different breast components and to more realistic radiation dose estimates, obtained with models based on real patient data.[12–16] With these 3D image datasets, the average breast glandular fraction (i.e., breast density [BD]) was found to be ~15%–20%,[17] and the average thickness of the skin layer was found to be about 1.5 mm.[18]

In addition to the overall lower BD, studies have also shown that the fibroglandular tissue is not distributed homogeneously throughout the breast but instead tends to concentrate in certain regions. This was shown for both uncompressed[19–22] and, recently, for compressed breasts,[23] by simulating the tissue displacement due to the mechanical compression during mammography and DBT. This new understanding of the more typical internal breast tissue distribution led to the realization that the current breast dosimetry models result, on average, to an overestimation of the mean glandular dose during mammography and DBT.[20–21,24] Furthermore, previous efforts for the development of dosimetry models for mammography and DBT mostly considered only the cranio-caudal (CC) projection, thus not accounting for possible differences in absorbed dose due to, for example, the presence of the pectoralis muscle in the medio-lateral-oblique (MLO) field of view. In the few studies where the pectoral muscle was accounted for,[9,25] it was simply modeled based on subjective opinion of a single expert reader.

Therefore, a new breast model that better describes the heterogeneous distribution of the fibroglandular tissue throughout the compressed breast, for both views, is needed.

In this study, computational phantoms of compressed breasts are presented, which reflect the heterogeneous distribution of the fibroglandular tissue within the breast as derived from mathematically compressed breast CT images, and validated in terms of their appropriateness for breast dose estimation. These phantoms, which may be used for dose estimates in mammography and DBT, will be made available upon reasonable request.

2 | MATERIALS AND METHODS

The phantoms were developed starting from the realistic binary shapes of compressed breasts, generated for the two views commonly used in mammography and DBT, CC and MLO, and for multiple breast thicknesses. These binary shapes were filled with voxels of adipose/fibroglandular tissue mixture, whose relative prevalence varies throughout the breast volume and whose magnitude depends on the overall glandular fraction to be modeled. For the MLO view, the pectoral

muscle was also modeled and included in the breast shape. To guide the heterogeneous distribution of fibroglandular tissue, a patient-based model of the breast parenchyma was used, which describes the amount of fibroglandular tissue that can be found in different locations of a compressed breast. The methods described can be used to generate multiple phantoms, for both the CC and MLO compression, covering a range of breast thicknesses and glandular fractions.

Two validation steps were performed to assess the appropriateness of the developed phantoms. First, a sensitivity analysis of the mean glandular dose (D_g) due to variations in the pectoral muscle medio-lateral thickness profile in the MLO view was performed, for various breast thicknesses and glandular fractions, using Monte Carlo (MC) simulations. Second, the spatially varying internal distribution of fibroglandular tissue, and the method to incorporate it in the phantoms, was validated, from a dosimetric perspective. For this, the average dose predictions using the proposed phantoms were compared against a set of patient-based phantoms involving the actual fibroglandular tissue distribution in patient breasts. In addition, these estimates were compared to those obtained using a homogeneous breast tissue model similar to those currently used for breast dosimetry.

2.1 | Compressed breast shapes

Binary shapes of compressed breasts were obtained using a previously developed patient-based 3D model of breasts undergoing mammography and DBT.[26] A dataset of compressed breast surfaces was first obtained by imaging a group of women with structured light surface imaging, performed in parallel with a DBT exam. Subsequently, the breast surface between the compression paddle and the support table from each patient was characterized with a set of equidistant arcs, which was then reduced to a smaller set of linearly independent parameters via principal component analysis (PCA). Finally, the results of the PCA were combined with a 2D model of the projected outer breast shape obtained separately from patient CC- and MLO-view mammograms,[27] to generate the final 3D models of compressed breasts. This was achieved in a sequential procedure, by first generating, for a given thickness, the 2D average breast shape based on mammography, and subsequently the average set of PCA parameters defined by the 3D surface model. Using these PCA parameters, the set of arcs describing the breast curvature was reconstructed, and the 3D shape of the breast surface was built at each point of the 2D projection through interpolation.[27] For the MLO shape, the projection of the edge of the pectoralis muscle visible in the MLO view was also characterized from the MLO-view mammograms, resulting, together with the outer shape, in models of the projection of the average muscle and its variation with breast thickness and size.

This binary shape model was used to generate a set of CC and MLO shapes of compressed breasts for 13 different breast thicknesses, with the PCA parameters chosen to represent the average surface shape, for a given thickness, within the study population.[26] The values for the 13 thicknesses were chosen to be 10 mm, and then 15–125 mm with 10-mm steps. However, as the relationship between the PCA eigenvalue that defines the thickness and the equidistant arcs is approximate, the model generates actual shapes with thickness that can actually vary from the desired one by up to 2 mm. For example, the thinnest breast was desired to be 10-mm thick, but the PCA-based method resulted in a shape with an actual thickness of 12 mm, which therefore defined the thinnest model used.

Each shape is represented by a 3D binary image with a cubic voxel size of 1 mm, with breast voxels set to 1 and voxels outside the breast set to 0. Before filling the breast voxels with the adipose/fibroglandular tissue mixture, the outer skin layer was included in the shape (inside the breast volume). To do so, the breast shapes were resized to a voxel size of 0.5 mm through nearest neighbor interpolation, and a 3-voxel layer (corresponding to 1.5 mm[18]) was included in the shape through morphological erosion.

2.2 | Fibroglandular tissue model

A previously developed fibroglandular tissue model was used for the internal tissue composition definition.[23] The model was obtained by characterizing the fibroglandular tissue distribution in patient breasts imaged using 3D dedicated breast CT. Briefly, 88 patient (mean age: 57-year old; range: 49–75) breast CT images were segmented into the major breast tissue types (skin, adipose, and fibroglandular tissue),[28] and simulated mechanical compression was applied to mimic the positioning for mammographic acquisition in the CC and MLO views.[29] From these compressed, patient-based phantoms, the average fibroglandular distributions in the axial, coronal, and sagittal directions were characterized separately by analyzing how the glandular fraction is spatially distributed throughout the breast. This resulted in three density distributions (one for each anatomical direction) that represent the heterogeneous concentration of the fibroglandular tissue within an average compressed breast.

As further detailed in Ref. [23], the fibroglandular tissue tends to be more concentrated in the anterior and caudal regions of the breast, with a symmetrical distribution in the medio-lateral direction for the CC compression, and a shifted distribution, by about 10% toward the lateral direction, for the MLO compression. As reported in Ref. [23], no significant differences in the

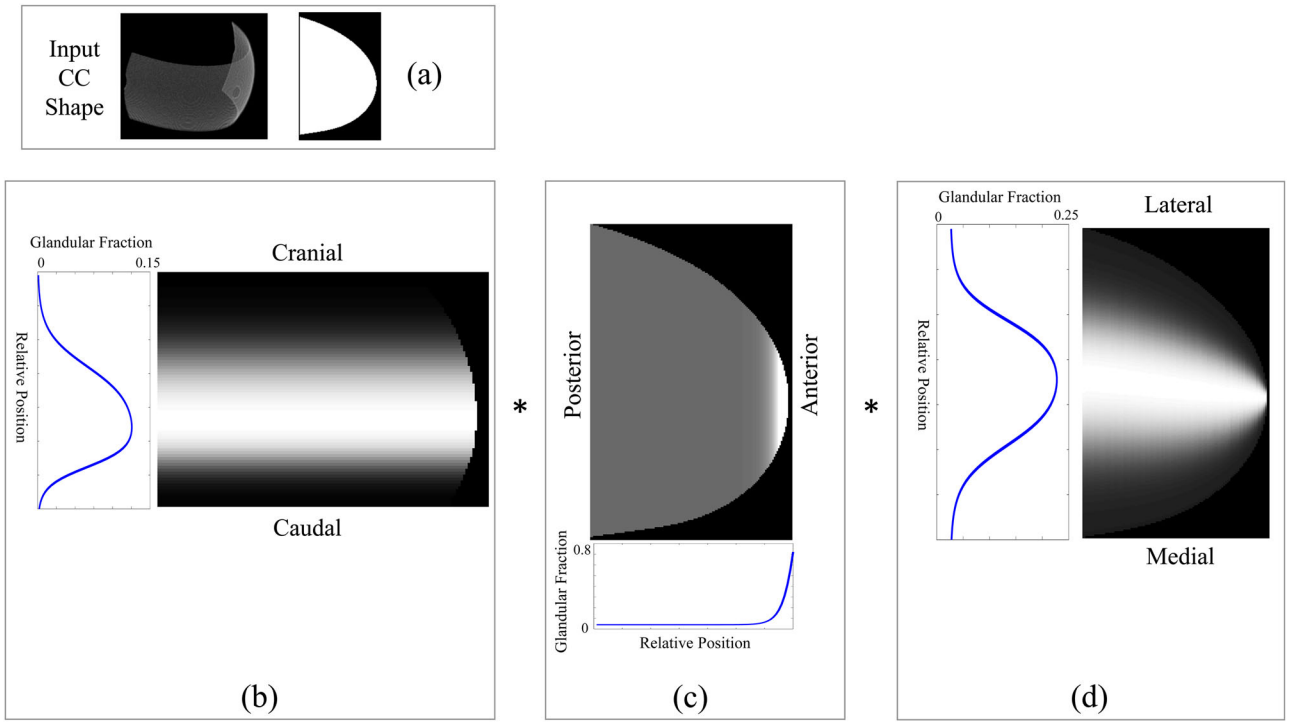

FIGURE 1 Initial step of the development of the cranio-caudal (CC) phantoms. The input compressed breast shape (panel a, three-dimensional [3D] rendering and central slice) was used to generate three initial breast density maps (panels b–d), each obtained by replicating the respective fibroglandular tissue probability density function within the shape.

shape of the distributions were observed for breasts of different sizes, thicknesses, and overall glandular fractions.

These three distributions were used to define the internal tissue distributions for the phantoms developed in this work, as described in the next sections.

2.3 | Cranio-caudal phantoms

The method to generate the heterogeneous CC phantoms requires two inputs: a breast shape compressed along the CC direction, and the desired overall glandular fraction of the final phantom. The latter represents a constraint in the phantom generation process, which forces each voxel to assume a value of the relative adipose/fibroglandular tissue prevalence in the mixture so that the desired global glandular fraction is obtained. To achieve this, three copies of the input binary breast shape (Figure 1a) were made, and each was filled with fibroglandular/adipose tissue mixture according to one of the three probability distributions of the fibroglandular tissue model (Figure 1b–d). In other words, the three density distributions of the model described in the previous section, for the CC case, were separately replicated in a copy of the compressed breast shape. The CC distribution was replicated in the compressed breast shape from paddle to support table, without accounting for the skin layer position (Figure 1b). This was done to avoid shrinking the input distribution in the locations where the breast thickness varies, which would have caused an unrealistic fibroglandular tissue distribution in regions close to the nipple (where the fibroglandular tissue tends to concentrate uniformly and with high density), and especially close to the outer portion of the breast. The same process was applied for the anterior–posterior distribution (Figure 1c), to avoid an unrealistic fibroglandular tissue distribution in regions close to the skin layer. The lateral–medial distribution (Figure 1d), instead, was filled in the breast shape from skin to skin, to more accurately reflect the symmetrical fibroglandular tissue pattern in this direction, as identified in Ref. [23].

The three maps were then multiplied together and normalized to a maximum of unity. This resulted in a 3D map, with voxels representing the relative concentration of fibroglandular tissue at each breast location (Figure 2).

The voxel values over the whole breast were then filled according to this 3D map to generate phantoms with the desired global glandular fraction. This was obtained by multiplying the 3D map with a factor x, obtained by minimizing the following function:

$$f(x) = \left| \frac{1}{N} \sum_{i=1}^{N} minimum(P_i \times x,\ 100) - G \right| \quad (1)$$

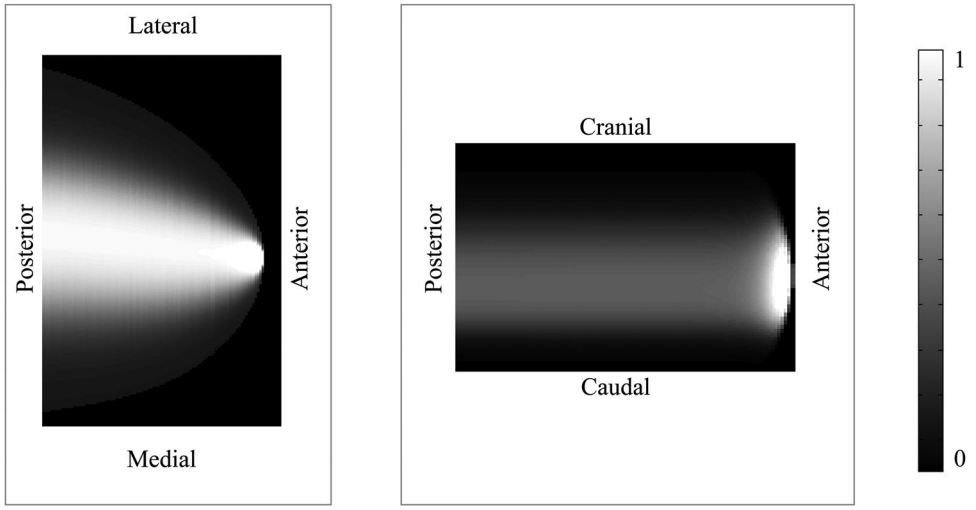

FIGURE 2 Three-dimensional probability map of the fibroglandular tissue concentration (shown for two views), obtained by the product and the normalization of the three separate distributions shown in Figure 1

where P_i is a voxel of the 3D map (with N voxels in total), and G the desired global glandular fraction. This function models the error in glandular fraction over the parameter x, with the *minimum* operator used as a constraint on the glandular fraction assigned to each voxel, which cannot exceed 100%. It was minimized using a nonlinear, derivative-free method based on the Nelder–Mead simplex algorithm, which iteratively moves toward the minimum by updating simplex directions in various points of the function.[30] Once the optimal value of x according to $f(x)$ is found, it was multiplied by the probability map, and the voxel values that exceed the maximum possible voxel-wise glandular fraction (i.e., 100%) were cropped to 100%. This led to a simultaneous adjustment of all voxel values that result in the desired global glandular fraction.

Through the process described in this section, phantoms with any desired thickness and global glandular fraction can be generated, with the latter being distributed heterogeneously throughout the whole breast volume.

2.4 | Medio-lateral-oblique phantoms

The methodology applied to generate the heterogeneous MLO phantoms was similar to that used for the CC phantoms. The fibroglandular tissue model was given by the MLO density distributions from Ref. [23], as described in Section 2.2. An example of the input compressed breast shape used is shown in Figure 3a. As can be seen, the MLO breast shapes include both the breast and the pectoral muscle, whose planar coordinates (x, y) in the axial view are provided with the input breast shape.

To generate the MLO phantoms, the pectoral muscle was separated from the rest of the breast volume, and the latter rotated counter-clockwise to align the pectoral muscle line to that of the chest wall edge (Figure 3a). This was done to align the outer breast shape of the MLO model with that of the fibroglandular tissue distribution. As for the CC model, the internal tissue distribution was defined by replicating the three unidirectional distributions in three copies of the breast volume, and then combining them via multiplication and normalizing them to a unity maximum (Figure 3b–d). The breast volume was then rotated back to its initial position and reunited with the volume that includes the pectoral muscle.

Based on the appearance of MLO mammography and DBT images, the cross section of the pectoralis muscle can be approximated as a triangle, located adjacent to the posterior side of the breast. However, the thickness of the pectoralis muscle in the MLO direction cannot be determined from these images due to the lack of true 3D information in the images of the breasts under compression. The shape of the pectoral muscle was therefore incorporated by modeling the pectoralis muscle with a pyramidal shape (with the cross section based on the average real shape of the pectoralis in MLO mammograms[27]) of varying lateral–medial thickness. This was defined as an additional input parameter for the phantom generation process, as the ratio between the maximum thickness of the pectoral muscle and the total compressed breast thickness (excluding the 1.5-mm skin layer) (Figure 4). The pectoral muscle was therefore defined as a pyramid with the vertex at the chest wall in-line with the nipple (or most anterior point of the breast), the base at the cranial edge of the breast volume, and the thickness at the base set according to the input ratio (Figure 5). The remaining chest wall tissue voxels not occupied by the added pectoralis muscle were filled with breast tissue by extrapolating the normalized 3D distribution along the anterior–posterior direction (Figure 5c). Finally, similarly as performed in a

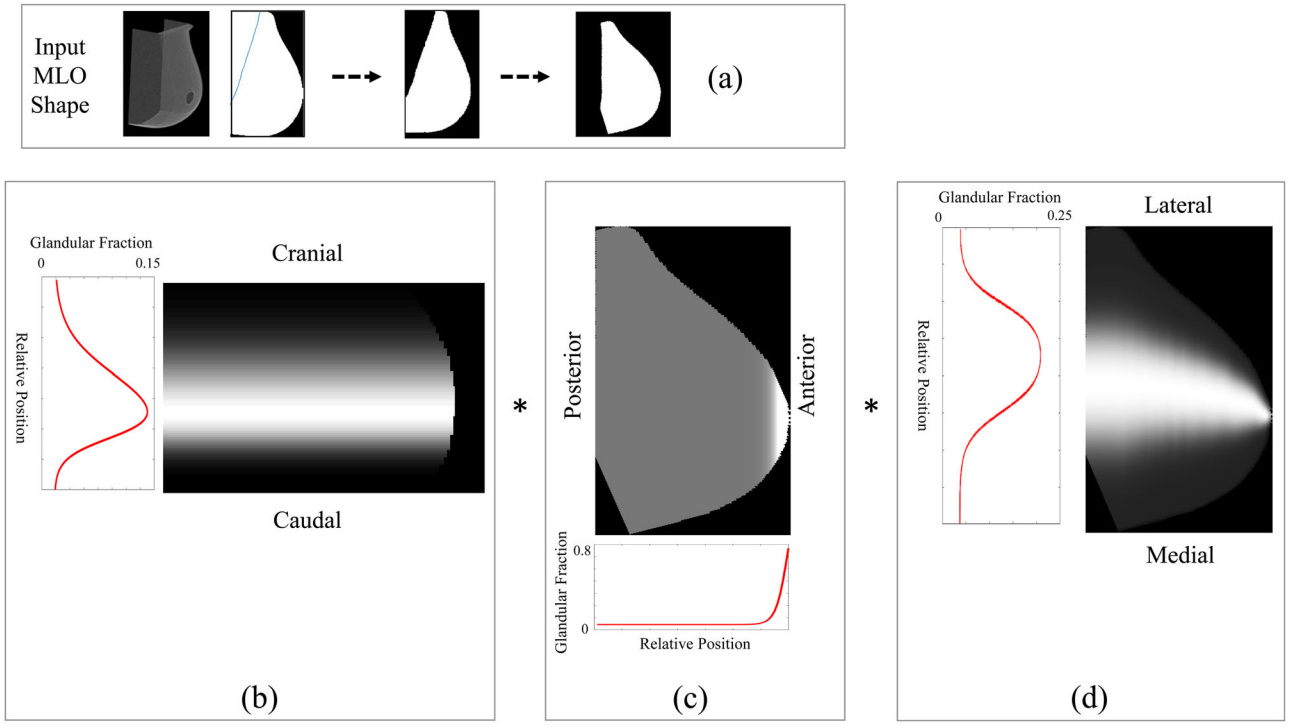

FIGURE 3 Initial step of the development of the medio-lateral-oblique (MLO) phantoms. The breast volume from the input compressed shape was first separated from the chest wall and rotated by the angle between the pectoral muscle line and the vertical axis (panel a). The reoriented shape was then used to generate three initial breast distribution maps (panels b–d), each obtained by replicating the fibroglandular tissue distributions within the shape.

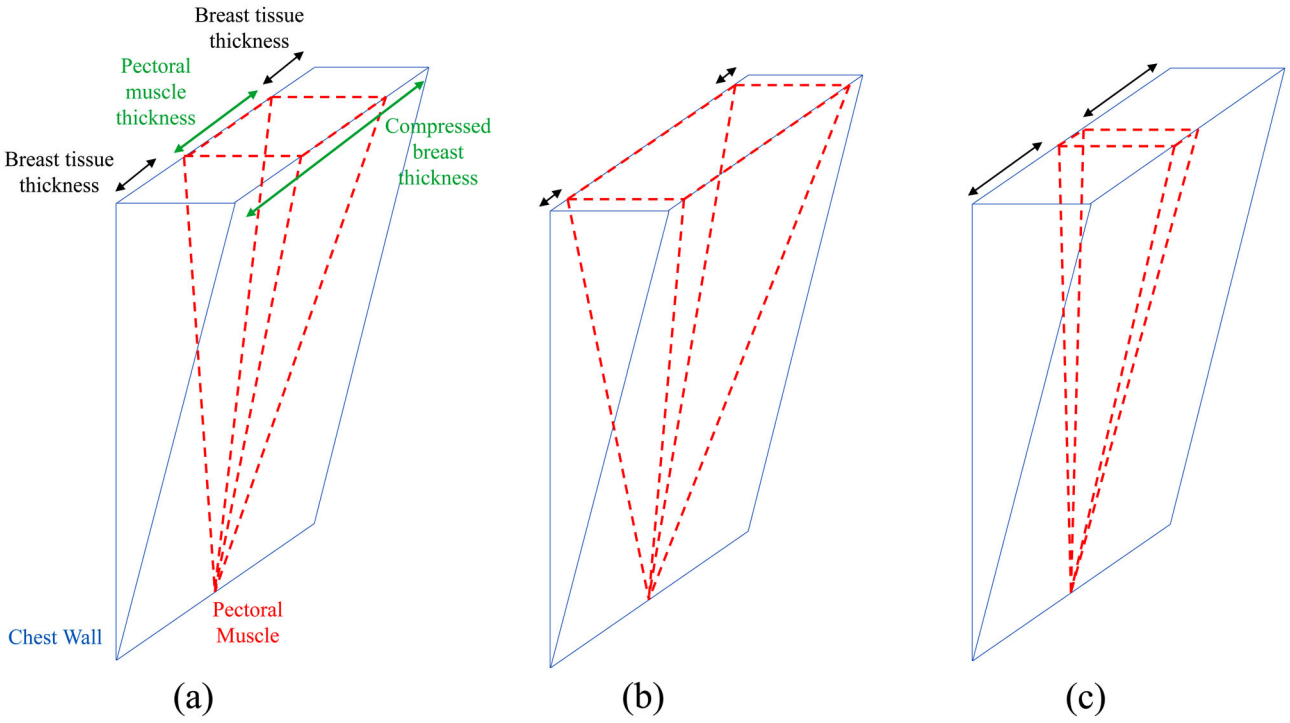

FIGURE 4 (a) Schematics of the pectoral muscle developed and included in the medio-lateral-oblique (MLO) phantoms, modeled by a pyramidal shape, with the width varying according to the defined ratio between the muscle and the breast volume thickness. Parts (b) and (c) show the schematic examples of two different pectoral muscles, defined for large and small values of this ratio.

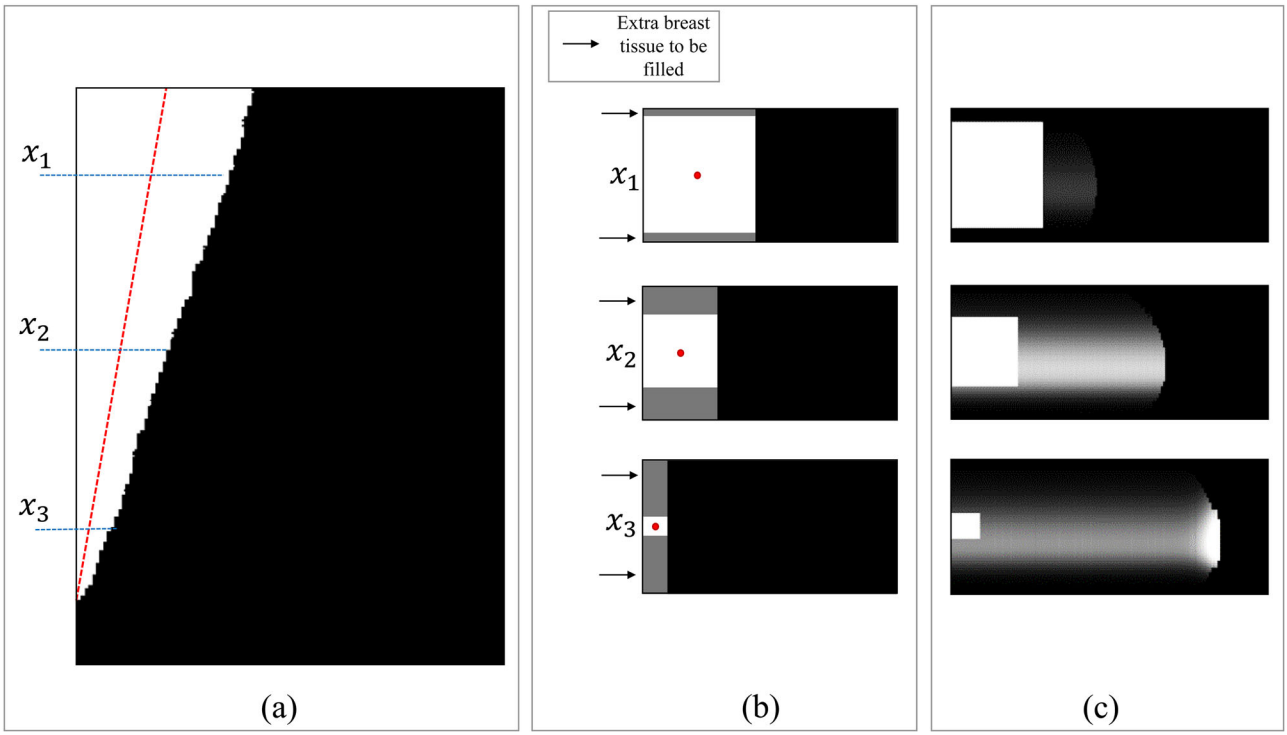

FIGURE 5 (a) The pectoral muscle was generated by first identifying the pectoral midline (dotted line), defined as the line that joins the lowest point of the chest wall with the center of its upper cross-section. (b) The pectoral muscle was then created around this midline (represented as a dot in the cross-sectional images), with the width in the lateral–medial direction set according to the desired input ratio between the muscle and the breast thickness. (c) The remaining chest wall tissue voxels not occupied by the added pectoral muscle were filled with breast tissue, by extrapolating the normalized probability along the anterior–posterior direction.

previous study for breast dosimetry in DBT,[9] the most cranial part of the MLO phantoms was modeled with a prism with triangular section. This part was not present in the original breast shapes, as it is located outside the mammographic field of view, but was included to allow for an improved realism of the phantoms when used to simulate DBT projections (i.e., when the projection angle differs from 0°). The internal voxels of this added region were assigned a value of adipose/fibroglandular tissue mixture by extrapolating the values of the nearby voxels.

An example of the final representation of the normalized MLO phantoms is shown in Figure 6.

Once all voxels of the input shape were assigned with a value to either represent the pectoralis muscle or skin (both of these being discrete indices), or breast voxels (continuous values between 0 and 1), the latter were iteratively filled with adipose/fibroglandular tissue mixture according to the normalized 3D map, until the input desired glandular fraction is reached, as performed for the CC case.

Through this process, MLO phantoms with multiple combinations of input parameters (breast thickness, overall glandular fraction, and pectoral muscle latero-medial thickness) can be generated. With the aim of reducing the complexity of this framework, we investigated the effect of the pectoral muscle thickness on dose estimates, as described in the following section.

2.5 | Pectoral muscle thickness sensitivity analysis

The effect of the pectoral muscle latero-medial thickness on the radiation dose in the MLO phantoms was studied with MC simulations. The mean glandular dose and its variability over different pectoral muscle thicknesses was estimated, and the most appropriate "average" geometric model for the muscle shape, from a dosimetric point of view, was determined.

The MC simulation code used was previously developed and validated. It is based on the Geant4 toolkit (release 10.07, February 2021)[9,20,31,32] and designed for breast dosimetry purposes. For simulations, different MLO phantoms were generated for multiple breast thicknesses (27, 56, and 85 mm), overall glandular fractions (5%, 15%, and 45%), and ratios between the maximum thickness of the pectoral muscle and the total compressed breast thickness (10%–90%, in steps of 10%). For each phantom, the muscle composition was specified as that of skeletal muscle according to ICRU Report 44.[33] In the simulation of mammographic image acquisition (0° projection), the X-ray source was located 67 cm above the detector, with the X-ray beam collimated to an area of 24 cm × 30 cm at the source-to-detector distance (Figure 7). The compression paddle and breast support table were defined as

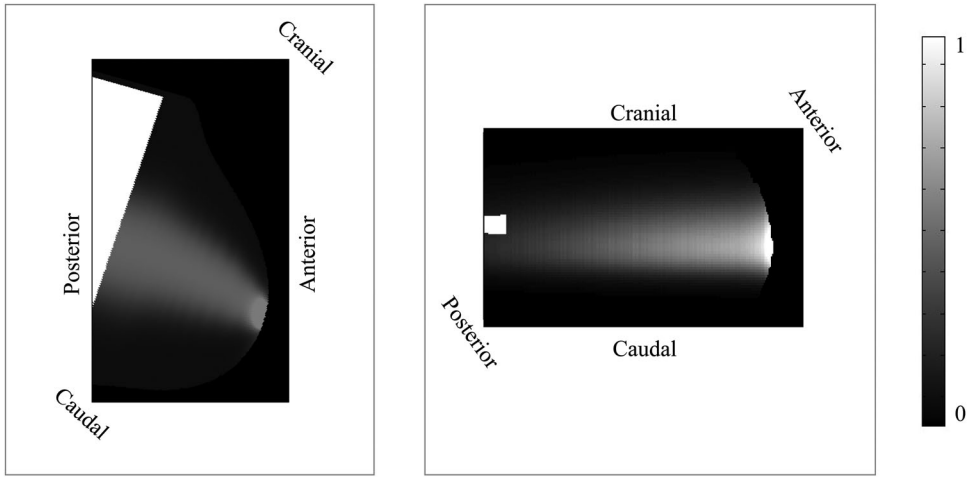

FIGURE 6 Three-dimensional probability maps of the fibroglandular tissue concentration (shown for two views), obtained by the product and normalization of the three separate distributions shown in Figure 3, with the pectoral muscle included

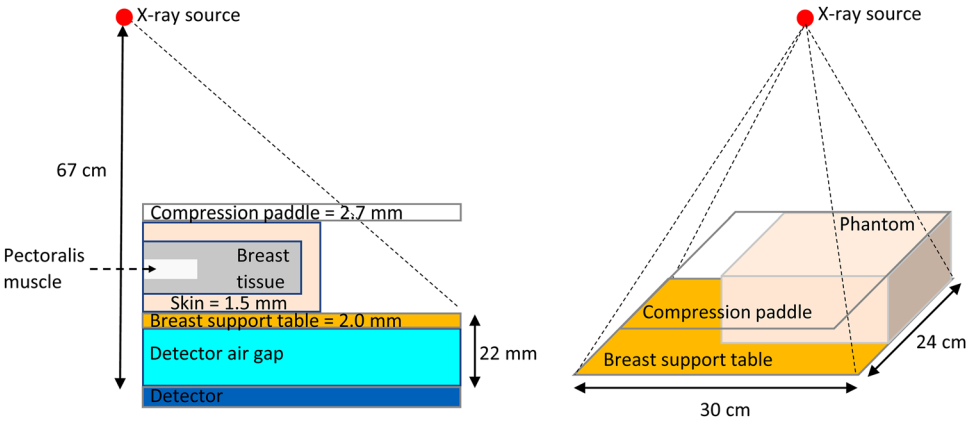

FIGURE 7 Schematics of the side and top views of the geometry defined in the Monte Carlo (MC) simulations

a 2.7-mm-thick layer of polyethylene terephthalate, and a 2-mm-thick layer of carbon fiber, respectively. The detector air gap was set to 2.2 cm. The heel effect was defined as the average of that measured on DM systems from five different vendors.[32] The border of the phantom was positioned aligned with the detector cranial and chest wall sides (Figure 7). Different spectra, generated following the TASMICSM-T model, were used according to each breast thickness.[34] The target/filter combination was tungsten/rhodium with 0.05-mm filter thickness for all simulations, but the tube voltage was set according to compressed breast thickness as follows: 26 kV (first HVL 0.436-mm Al, for breast thickness 27 mm), 29 kV (first HVL 0.464-mm Al, for breast thickness 56 mm), and 32 kV (first HVL 0.486-mm Al, for breast thickness 85 mm). These exposure settings were selected according to those used by the automatic exposure control for a clinical digital mammography system (Siemens Mammomat Inspiration, Forchheim, Germany).

For each phantom, 10^7 X-rays were simulated, with the resulting precision of the dose estimates calculated using the method of[35] and resulting in an uncertainty of less than 1%. These photons were followed until they were completely absorbed or left the simulation volume. The simulations were performed using the EPDL97 library[36] by selecting the Geant4 electromagnetic Physics List Option 4,[37] and the default cut range for photons was used.

As each voxel in the phantoms is a mixture of adipose and fibroglandular tissue represented by a glandularity g_i, the mean glandular dose was computed by recording each energy deposition event that occurred in each breast voxel i, and weighted by the corresponding G_i factor,[5] following the equation:

$$D_g = \frac{\sum_i \sum_j E_{i,j}^{dep} G_i\left(g_i, e\right)}{\sum_i \frac{Vg_i}{\frac{g_i}{\rho g} + \frac{(1-g_i)}{\rho a}}} \quad (2)$$

where E_{ij}^{dep} is the energy deposited in the voxel i during event j by a photon with energy e at the moment of the energy deposition, ρ_a and ρ_g are the adipose and fibroglandular tissue densities (equal to 0.93 and 1.04 g/cm^3, respectively),[2] V is the voxel volume (0.5 mm × 0.5 mm × 0.5 mm).

In the previous equation, the factor G_i for voxel i is given by

$$G_i(g_i, e) = \frac{g_i\left(\frac{\mu_{en}(e)}{\rho}\right)_g}{\left[g_i\left(\frac{\mu_{en}(e)}{\rho}\right)_g + (1 - g_i)\left(\frac{\mu_{en}(e)}{\rho}\right)_a\right]} \quad (3)$$

where $(\mu_{en}(e)/\rho)$ represents the mass energy absorption coefficients for X-rays of energy e in fibroglandular and adipose tissues (subscripts g and a, respectively).[5]

2.6 | Dosimetric evaluation of the internal heterogeneous tissue distribution

The heterogeneous distribution of fibroglandular tissue used to represent the inner breast tissue in the proposed phantoms was compared, from a dosimetric perspective, to patient-based compressed breast phantoms that include the actual distribution of the fibroglandular tissue in the breast. The dose estimates resulting from the proposed phantoms were also compared to those obtained using the homogeneous distribution now commonly used in breast dosimetry.

The patient-based phantoms were the same 88 phantoms described in Section 2.2, obtained by segmenting as many breast CT patient images into skin, fibroglandular, and adipose tissue, which were then mechanically compressed along both the CC- and the MLO-view directions. The patient-based phantom thicknesses ranged between 30 and 82 mm for the CC view, and 26–80 mm for the MLO view. Voxel size was 0.273 mm per side, and BD, by mass, varied between 2% and 70% (mean 20%, median 15%).

Given that the voxels in these patient phantoms were labeled as either skin, 100% adipose, or 100% fibroglandular tissue, BD was calculated as

$$BD = \frac{n_g\rho_g}{n_g\rho_g + n_a\rho_a} \quad (4)$$

where n_g and n_a are the total number of voxels classified as fibroglandular and adipose tissue, respectively, and ρ_g and ρ_a the corresponding densities (0.93 and 1.04 g/cm^3).[2]

To avoid any bias due to differences in breast shapes or skin thickness, and thus to provide an objective dosimetric evaluation only of the heterogeneous fibroglandular tissue distribution, the shapes of the patient-based phantoms were used here to generate the corresponding heterogeneous and homogeneous versions. That is, using the shapes of the 88 breast CT patient phantoms, another two sets of 88 phantoms each were generated. For the homogeneous case, the breast tissue voxels in the shape (i.e., those labeled as either fibroglandular or adipose tissue) were replaced by voxels containing a mixture of both materials with the corresponding BD by mass. For the heterogeneous phantoms, the breast tissue voxels were filled with adipose/fibroglandular tissue mixture according to the distributions described in Section 2.2, until reaching the corresponding BD. An example of these patient-based, heterogeneous and homogeneous phantoms used in the MC simulations are shown in Figure 8.

To increase the generalizability of the results, these heterogeneous phantoms were not generated from the exact density distributions reported in Ref. [23] and described in Section 2.2. Instead, the evaluation was performed using five fold cross-validation. Therefore, the 88 patient-based phantoms were randomly divided into five folds, the fibroglandular tissue distributions recalculated from four folds, and then used to fill the phantom shapes in the remaining fold. The process was repeated five times to cover all folds, resulting in the generation of the 88 heterogeneous phantoms.

The three derived groups of phantoms (patient-based, heterogeneous, and homogeneous, Figure 8), each composed of 176 cases (88 CC, 88 MLO), were used in MC simulations to estimate the normalized mean glandular dose (D_gN), which was estimated with the same MC simulation code used for the pectoral muscle sensitivity analysis described in the previous section.

For the segmented patient phantoms, which present discretized voxel values for the inner breast tissue (either 100% adipose, or 100% fibroglandular), the $D_gN_{Patient}$ was calculated from the total energy deposited in the fibroglandular tissue voxels, and normalized by the incident air kerma (AK) following the equation:

$$D_g\,N_{Patient} = \frac{\sum_i E_{dep}}{n_g\rho_g V} \cdot \frac{1}{AK} \quad (5)$$

$$AK = \sum_e \Phi_e e\left(\frac{\mu_{en}(e)}{\rho}\right)_{air} \quad (6)$$

where E_{dep} is the energy deposited in all the fibroglandular voxels, n_g the total number of fibroglandular tissue voxels, ρ_g the fibroglandular tissue density, V the voxel volume (0.273 mm × 0.273 mm × 0.273 mm for the patient-based breast CT phantoms), Φ_e the fluence for X-ray photon energy e, and $(\mu_{en}(e)/\rho)$ the mass energy absorption coefficients. The incident AK was calculated within a 3 cm × 3 cm surface placed in contact with the

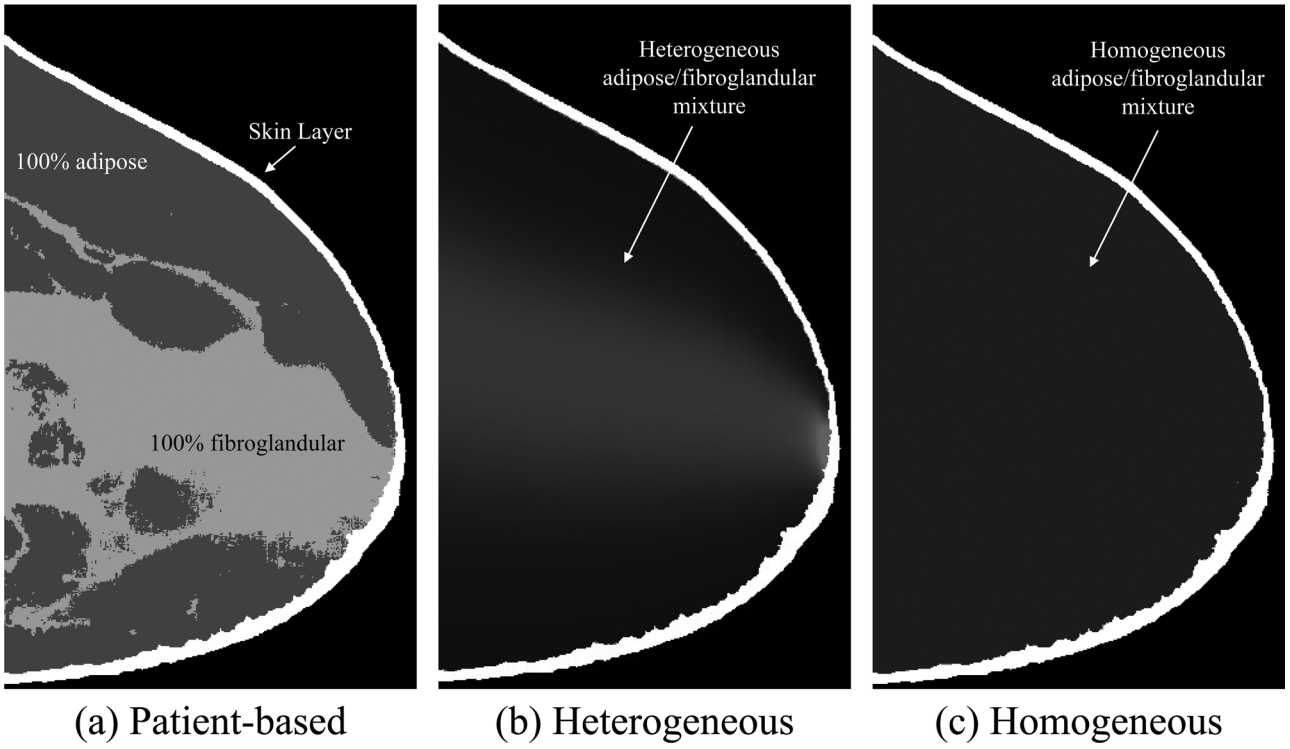

FIGURE 8 Examples of phantoms (central slice) used in the Monte Carlo (MC) simulations to estimate the D_gN values for (a) patient-based, (b) heterogeneous, and (c) homogeneous phantoms. All three examples contain the same overall glandular fraction (17%).

phantom, 6 cm from the chest wall, laterally centered, with the compression paddle in place.

On the other hand, as each voxel in the heterogeneous and homogeneous phantoms is a mixture of adipose and fibroglandular tissue represented by a glandularity g_i, the respective D_gN_{Hetero}, and D_gN_{Homo} were calculated as done in the pectoral muscle sensitivity analysis, and normalizing by AK:

$$D_g\,N_{Hetero/Homo} = \frac{\sum_i \sum_j E_{i,j}^{dep} G_i\left(g_i, e\right)}{\sum_i \frac{V g_i}{\frac{g_i}{\rho g} + \frac{(1-g_i)}{\rho a}}} \cdot \frac{1}{AK} \qquad (7)$$

For all simulations described in this section, the exposure settings were selected based on those set by the automatic exposure control of a clinical digital mammography system (Siemens Mammomat Inspiration, Forchheim, Germany) obtained from mammograms of real patients, with compressed thicknesses matching those of the phantoms used.

3 | RESULTS

The actual thicknesses for all breast shapes generated for this study, together with breast volume and largest cross-sectional area, are reported in Table 1.

Using the developed methodology, compressed breast phantoms for the CC and MLO views can be generated for multiple breast thicknesses, and any value of overall glandular fraction and maximum pectoral muscle thickness. As an example, Figure 9 shows eight different phantoms (four CC, top row, and four MLO, bottom row) generated for four compressed breast thicknesses, and two overall glandular fractions. As can be seen, the fibroglandular tissue is distributed heterogeneously within the breast according to the patient-based density model of[23] briefly described in Section 2.2, and its amount in different breast regions depends on the overall desired glandular fraction.

3.1 | Pectoral muscle thickness sensitivity analysis

Figure 10 presents the mean glandular dose (D_g) obtained in the MC simulations for phantoms with different thicknesses and glandularities as a function of the maximum thickness of the pectoral muscle in the phantom. In all cases, the relative variation was less than 1%. As expected, D_g depends strongly on the compressed breast thickness, and on the BD to a smaller degree. However, it is almost completely insensitive to the thickness profile of the muscle. Specifically, for all conditions evaluated, the average coefficient of variation (COV) was 0.48% (min: 0.28%; max: 0.77%).

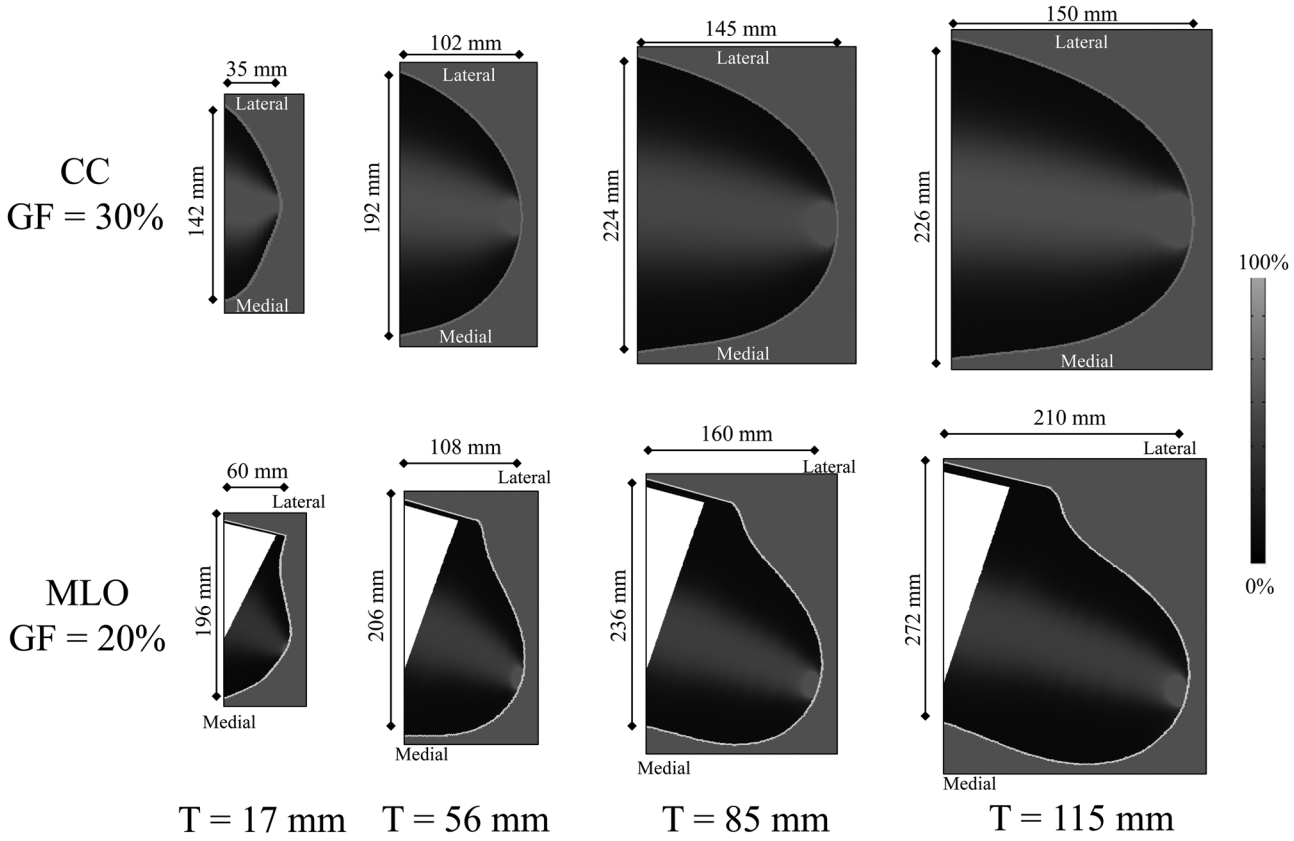

FIGURE 9 Central slices through eight different examples of cranio-caudal (CC) (top row) and medio-lateral-oblique (MLO) phantoms (bottom row) generated for four compressed breast thicknesses (*T*), and two overall glandular fractions (*GF*)

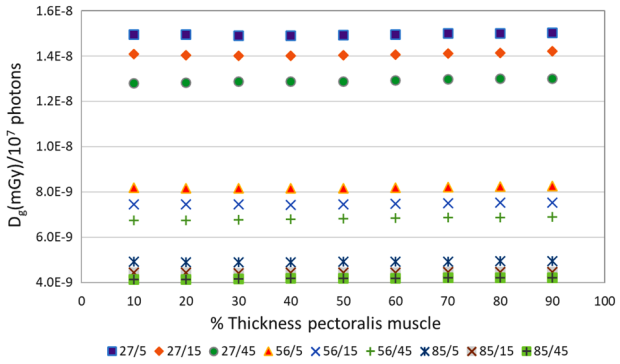

FIGURE 10 D_g as a function of the pectoral muscle thickness (defined as the percentage of the thickest portion of the muscle relative to the total breast tissue thickness) in the phantom for different configurations of breast thickness (in mm)/glandularity (in %)

Figure 11 shows the relative deviations of D_g from their respective mean values as a function of the relative pectoral muscle thickness. For most breasts, the relative deviations cross zero when the pectoral muscle thickness is 45%–65% of the total breast thickness (horizontal axis in Figure 11). The results for each breast thickness and glandularity were fit to a quadratic ($R^2 > 0.82$), also shown in the figure, and the mean values of the corresponding polynomial roots were found to be 8% and 58%. Therefore, if the pectoral muscle to total breast tissue thickness ratio was set to 58%, the MLO model would result in a relative deviation in D_g of less than 0.5% for breasts with any other pectoral muscle thickness. Therefore, this pectoral muscle thickness is the one used in the rest of the study.

3.2 | Dosimetric evaluation of the internal heterogeneous tissue distribution

When the average D_gN for the heterogeneous fibroglandular tissue distribution was compared to that of the phantoms with actual patient-based tissue distribution, similar results were found, and both were, on average, over 30% lower than the D_gN estimated with the homogeneous models. As shown in Figure 12 (top row), in the CC view the homogeneous model overestimated the $D_gN_{Patient}$ by a mean factor of 1.43 (range: 0.79–1.90, Wilcoxon signed rank test $p < 0.0001$), whereas the heterogeneous model underestimated the $D_gN_{Patient}$ by a mean factor of 0.95 (range: 0.45–1.29, Wilcoxon signed rank test $p = 0.0004$). For the MLO view, Figure 12 (bottom row) shows that the homogeneous model overestimated the $D_gN_{Patient}$ by a mean factor

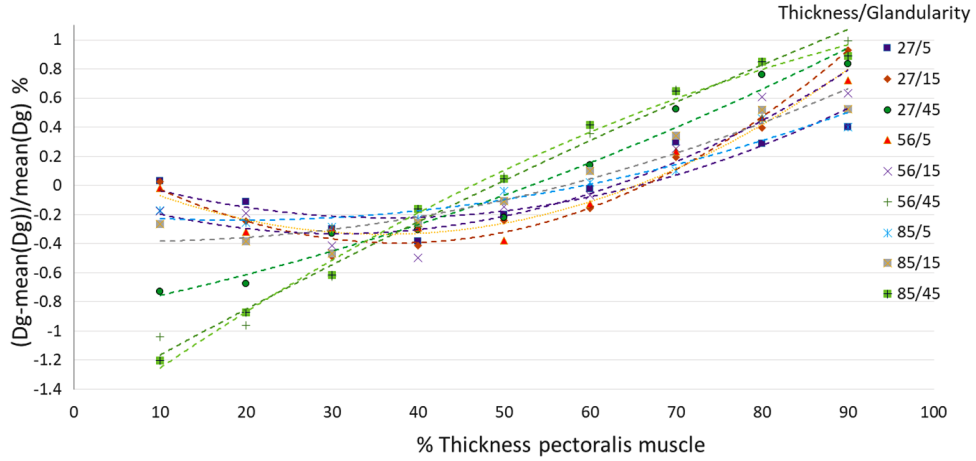

FIGURE 11 Normalized deviation of the D_g as a function of the maximum thickness of pectoral muscle (defined as the percentage of the total breast thickness occupied by the pectoral muscle at its thickest section) included in the phantom for different configurations of breast thickness and glandularity. The smooth curves are the quadratic fits for each normalized deviation of the D_g as a function of the pectoral muscle thickness.

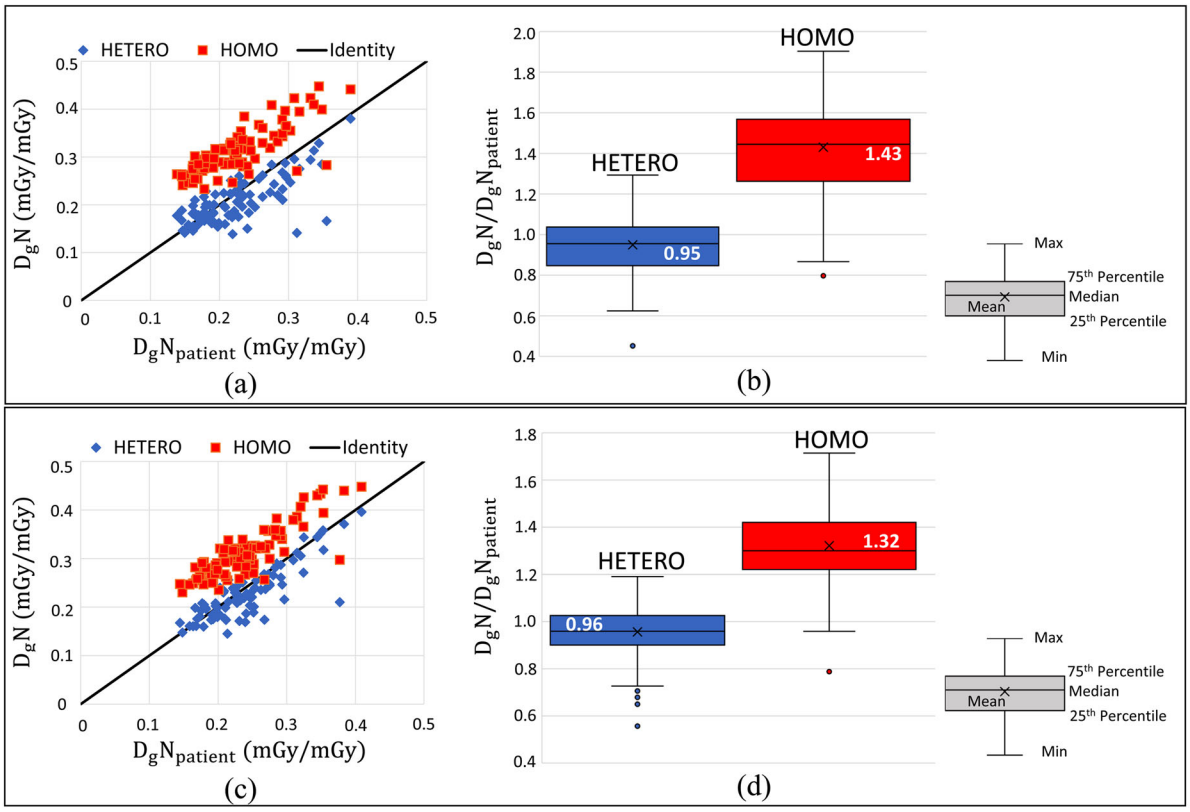

FIGURE 12 Top row: (a) comparison of the estimated D_gN values for the homogeneous and heterogeneous models to the corresponding D_gN of the patient-based breast computed tomography (CT) phantoms for the cranio-caudal (CC) view, (b) box–whisker plot of the D_gN ratios of the homogeneous and heterogeneous model to patient D_gN for the CC view. Bottom row: (c) comparison of the estimated D_gN values for the homogeneous and heterogeneous model to the corresponding D_gN of the patient-based breast CT phantoms for the medio-lateral-oblique (MLO) view; (d) box–whisker plot of the D_gN ratios of the homogeneous and heterogeneous model to patient D_gN for the MLO view

of 1.32 (range: 0.79–1.71, Wilcoxon signed rank test $p < 0.0001$), whereas the heterogeneous model underestimated the $D_gN_{Patient}$ by a mean factor of 0.96 (range: 0.56–1.19, Wilcoxon signed rank test $p = 0.0004$).

3.3 | Developed phantoms

A set of phantoms representing the most common glandular fraction values[17] in patient breasts was generated.

TABLE 1 List of thicknesses, volumes, and cross-sectional areas for the 13 generated binary breast shapes

Shape no.		1	2	3	4	5	6	7	8	9	10	11	12	13
Thickness (mm)	CC[a]	12	17	27	36	46	56	66	75	85	95	105	115	124
	MLO[b]	12	17	27	36	46	56	66	76	85	95	105	115	125
Area (cm^2)	CC[a]	29	35	52	77	109	146	183	218	248	268	273	258	220
	MLO[b]	89	94	105	125	149	181	216	256	298	343	389	434	477
Volume (ml)	CC[a]	30	53	131	262	467	748	1095	1474	1873	2230	2468	2505	2240
	MLO[b]	100	151	273	430	651	951	1322	1786	2307	2945	3653	4430	5246

[a]Cranio-caudal.
[b]Medio-lateral-oblique.

These phantoms were generated for 13 different breast thicknesses (Table 1), each with 6 overall glandular fractions (1%, and then 10%–50% with 10% steps), with the breast compressed for both the CC and MLO views. This results in a total of 78 phantoms per view, covering a wide range of breast densities and thicknesses. Each voxel in the phantoms has isotropic dimensions of 0.5 mm and is labeled with a numerical integer value that represents a different component: fibroglandular tissue percentage concentration (0–100), air (101), skin (102), and, for the MLO case, pectoral muscle (103). These phantoms will be made available upon reasonable request.

4 | DISCUSSION

In this study, we described a methodology to generate heterogeneous breast phantoms for dosimetry in mammography and DBT. These phantoms were developed from realistic breast shapes compressed along both the CC and MLO views and were filled with adipose/fibroglandular tissue mixtures according to a patient-based model of the breast parenchyma in compressed breasts. With the developed methodology, heterogeneous breast phantoms of different thicknesses can be generated for any desired overall glandular fraction and, for the MLO case, thickness of the pectoral muscle.

When validating these phantoms from a dosimetric perspective, they showed high agreement with the patient-based phantoms containing the actual distribution of the fibroglandular tissue in the breast as seen in compressed breast CT images, for both the CC and MLO views. This suggests, therefore, their adequacy for use in dosimetric simulations in mammography and DBT. It should be noted that adequate model dosimetry phantoms are those that can be used to represent the population of patient breasts of equal breast thickness and density. Therefore, the dose to the model phantoms should approximate the average of the patient population dose, but it cannot equate to each specific individual patient dose. Given the strong influence that the location of the fibroglandular tissue in the breast has in the dose, it would be impossible for a single breast model to replicate the individual dose received by patient breasts. As a result, the aim of a model dosimetry phantom is for the median or mean of the ratio between model and patient breasts to be close to unity, not for the spread of this ratio to be minimized.

The more accurate dose estimates obtained with the developed heterogeneous phantoms could correct for the overestimation of dose provided by the currently used homogeneous model (~30%–40%). However, it should be noted that this reduction in dose does not necessarily imply that the dose-induced risk is reduced by the same amount. Therefore, current risk models in

breast dosimetry may also need to be updated, to better reflect the improved, more realistic dosimetric results obtained.

When performing the MC simulations to validate the heterogeneous distribution of the proposed phantoms, the shapes of the patient-based compressed breast CT phantoms were used, as opposed to the shapes derived from mammograms described in Section 2.1. This choice was made to assess the similarity of the proposed heterogeneous distribution with the patient phantoms and with the corresponding homogeneous models, without introducing any other source of potential bias, such as the external breast shape. In other words, for these MC simulations, only the internal breast tissue distribution changed between the three groups of phantoms (heterogeneous, patient-based, and homogeneous), allowing for the objective validation of the proposed heterogeneous fibroglandular tissue distribution.

Using MC simulations, the mean glandular dose was observed to be only slightly sensitive to the pectoral muscle thickness profile, as in all cases COV values of less than 1% were obtained. These low COV values can be explained by the symmetrical position of the pectoral muscle within the phantom, as the decrease in the energy deposited seems to be closely compensated by the decrease in fibroglandular tissue mass. We concluded that an appropriate model value for the thickest portion of the muscle in an "average breast" under compression in the MLO view is equal to 58%. This value was determined considering the geometry defined for the muscle, and the fact that the pectoral muscle probably occupies the majority of the breast tissue space, in general, at the cranial end of the image.

It should be noted that, for the pectoral muscle thickness sensitivity analysis, only three shapes with representative compressed thicknesses spanning the range of breast thicknesses usually encountered clinically were used (27, 56, and 85 mm). Although additional compressed breast thicknesses might be evaluated in the future, we do not expect relevant changes in the results obtained, as in all cases the relative variation introduced by different pectoral muscle thicknesses was less than 1%.

The heterogeneous phantoms reported herein were validated both in terms of internal tissue distribution, and of pectoral muscle thickness for the MLO case. Considering the good average agreement with patient data, and the negligible effect of the pectoral muscle thickness on the mean glandular dose, the proposed phantoms hold the potential to improve radiation dose estimates in mammography and DBT.

Although the appropriateness of the new heterogeneous phantom was evaluated only with X-ray spectra that corresponded to those that would be used clinically for each breast thickness, the results found here could be expected to generalize to mismatches between compressed breast thickness and X-ray spectrum. This is because if the spectrum used were too soft for the breast thickness, the falling dose profile from top to bottom of the breast would be further accentuated, increasing the dose overestimation by the homogeneous model even further and faster than that for the heterogeneous model. If the X-ray spectrum were too hard, then both models would converge to the real patient dose in the limit of when the dose distribution were perfectly uniform.

The limitations of the developed phantoms are mainly related to the fibroglandular tissue model, which might be improved through the refinement of the mechanical compression simulation (as detailed in Ref. [23]), and to the compressed binary breast shapes, whose realism may be further improved through the acquisition and analysis of additional cases. Another limitation is having assumed that the pectoral muscle is symmetrical about the breast thickness centerline. However, given the lack of information on the vertical position of the muscle on a per-acquisition basis, it would be impossible to select the correct model to use for any given breast image acquisition. In other words, we will only have enough information during breast dosimetry calculations to use one single muscle model.

The validations performed present the limitation of having used a single geometric system definition for all MC simulations. However, the relatively small differences in the geometry of all the currently available commercial systems will most likely not contribute to generating significant differences in our results. Finally, all simulations were performed with the X-ray source positioned for mammography (equivalent to also 0° DBT projection), but given the already low effect found, any further differences due to nonzero DBT angles are expected to be even smaller.[38]

Future work may include the enlargement of the breast CT phantom dataset used to generate the fibroglandular tissue model, the improvement of the compression simulation algorithm, and the investigation of additional methods to replicate the tissue model in the presented heterogeneous phantoms (e.g., through expectation-maximization methods that directly reconstruct the 3D joint probability of the fibroglandular tissue).

5 | CONCLUSIONS

Digital phantoms of compressed breasts undergoing mammography and DBT imaging, for both CC and MLO views, were developed reflecting the average heterogeneous distribution of the fibroglandular tissue that is found in the compressed patient breast. The phantoms, thanks to their improved realism, achieved more accurate mean dose estimates compared to the currently used homogeneous BD model, showing good

average agreement with patient-based data. Therefore, they can be used to improve radiation dose estimates in mammography and DBT.

ACKNOWLEDGMENTS

The authors would like to thank Dr. Paul Segars for his support in visualization and rendering of the compressed breast shapes used in this study. This research was supported in part by Grant R01CA181171 from the National Cancer Institute, National Institutes of Health, and Grant IIR13262248 from the Susan G. Komen Foundation for the Cure. The authors would like to thank the Comisión Sectorial de Investigación Científica (CSIC) under project C681 in Uruguay. The content of this manuscript is solely the responsibility of the authors and does not necessarily represent the official views of the National Cancer Institute, the National Institutes of Health, the Komen Foundation, or the Comisión Sectorial de Investigación Científica.

CONFLICT OF INTEREST

The authors declare that there is no conflict of interest that could be perceived as prejudicing the impartiality of the research reported.

DATA AVAILABILITY STATEMENT

The data generated in this study will be made available by the corresponding author upon reasonable request.

REFERENCES

1. Ewton J, Shalek R, Egan R. Estimated radiation dose during mammography. *Cancer Bull*. 1962;14:116-117.
2. Hammerstein GR, Miller DW, White DR, Masterson ME, Woodard HQ, Laughlin JS. Absorbed radiation dose in mammography. *Radiology*. 1979;130:485-491.
3. Dance DR. Monte Carlo calculation of conversion factors for the estimation of mean glandular breast dose. *Phys Med Biol*. 1990;35:1211-1219.
4. Wu X, Gingold EL, Barnes GT, Tucker DM. Normalized average glandular dose in molybdenum target-rhodium filter and rhodium target-rhodium filter mammography. *Radiology*. 1994;193:83-89.
5. Boone JM. Glandular breast dose for monoenergetic and high-energy x-ray beams: Monte Carlo assessment. *Radiology*. 1999;213:23-37.
6. Boone JM. Normalized glandular dose (DgN) coefficients for arbitrary x-ray spectra in mammography: computer-fit values of Monte Carlo derived data. *Med Phys*. 2002;29:869-875.
7. Dance DR, Sechopoulos I. Dosimetry in x-ray-based breast imaging. *Phys Med Biol*. 2016;61(19):R271-R304.
8. Dance DR, Young KC, van Engen RE. Estimation of mean glandular dose for breast tomosynthesis: factors for use with the UK, European and IAEA breast dosimetry protocols. *Phys Med Biol*. 2011;56:453-471.
9. Sechopoulos I, Suryanarayanan S, Vedantham S, D'Orsi CJ, Karellas A. Computation of the glandular radiation dose in digital tomosynthesis of the breast. *Med Phys*. 2007;34:221-232.
10. Feng SSJ, Sechopoulos I. Clinical digital breast tomosynthesis system: dosimetric characterization. *Radiology*. 2012;263(1):35-42.
11. Sechopoulos I, Feng SSJ, D'Orsi CJ. Dosimetric characterization of a dedicated breast computed tomography clinical prototype. *Med Phys*. 2010;37:4110-4120.
12. Bliznakova K, Sechopoulos I, Buliev I, Pallikarakis N. BreastSimulator: a software platform for breast x-ray imaging research. *J Biomed Graphics Comput*. 2012;2(1)1-14. doi:10.5430/JBGC.V2N1P1
13. Mettivier G, Bliznakova K, Sechopoulos I, et al. Evaluation of the BreastSimulator software platform for breast tomography. *Phys Med Biol*. 2017;62(16):6446-6466.
14. Sarno A, Mettivier G, Di Lillo F, Bliznakova K, Sechopoulos I, Russo P. Homogeneous vs. patient specific breast models for Monte Carlo evaluation of mean glandular dose in mammography. *Phys Med*. 2018;51:56-63.
15. Sarno A, Mettivier G, di Franco F, et al. Dataset of patient-derived digital breast phantoms for in silico studies in breast computed tomography, digital breast tomosynthesis, and digital mammography. *Med Phys*. 2021;48(5):2682-2693.
16. Caballo M, Fedon C, Brombal L, Mann R, Longo R, Sechopoulos I. Development of 3D patient-based super-resolution digital breast phantoms using machine learning. *Phys Med Bio*. 2018;63(22):225017.
17. Yaffe MJ, Boone JM, Packard NJ, et al. The myth of the 50-50 breast. *Med Phys*. 2009;36:5437-5443.
18. Huang SY, Boone JM, Yang K, Kwan ALC, Packard NJ. The effect of skin thickness determined using breast CT on mammographic dosimetry. *Med Phys*. 2008;35:1199-1206.
19. Huang SY, Boone JM, Yang K, et al. The characterization of breast anatomical metrics using dedicated breast CT. *Med Phys*. 2011;38(4):2180-2191.
20. Sechopoulos I, Bliznakova K, Qin X, Fei B, Feng SSJ. Characterization of the homogenous tissue mixture approximation in breast imaging dosimetry. *Med Phys*. 2012;39(8):5050-5059.
21. Hernandez AM, Seibert JA, Boone JM. Breast dose in mammography is about 30% lower when realistic heterogeneous glandular distribution are considered. *Med Phys*. 2015;42:6337-6348.
22. Arana Peña LM, Fedon C, García E, et al. Monte Carlo dose evaluation of different fibroglandular tissue distribution in breast imaging. Proc IWBI 2020. Vol 11513; 2020:115130G. doi:10.1117/12.2564278
23. Fedon C, Caballo M, García E, et al. Fibroglandular tissue distribution in the breast during mammography and tomosynthesis based on breast CT data: a patient-based characterization of the breast parenchyma. *Med Phys*. 2021;48:1436-1447. doi:10.1002/mp.1471
24. Sarno A, Mettivier G, Bliznakova K, Hernandez AM, Boone JM, Russo P. Comparisons of glandular breast dose between digital mammography, tomosynthesis and breast CT based on anthropomorphic patient-derived breast phantoms. *Phys Med*. 2022;97:50-58.
25. Sarno A, Mettivier G, Di Lillo F, et al. Normalized glandular dose coefficients in mammography, digital breast tomosynthesis and dedicated breast CT. *Phys Med*. 2018;55:142-148.
26. Rodríguez-Ruiz A, Agasthya GA, Sechopoulos I. The compressed breast during mammography and breast tomosynthesis: in vivo shape characterization and modelling. *Phys Med Biol*. 2017;62(17):6920-6937.
27. Rodríguez-Ruiz A, Feng SSJ, van Zelst J, et al. Improvements of an objective model of compressed breasts undergoing mammography: generation and characterization of breast shapes. *Med Phys*. 2017;44(6):2161-2172.
28. Caballo M, Boone JM, Mann RM, Sechopoulos I. An unsupervised automatic segmentation algorithm for breast tissue classification of dedicated breast computed tomography images. *Med Phys*. 2018;45(6):2542-2559.
29. García E, Fedon C, Caballo M, Martí R, Sechopoulos I, Diaz O. Realistic compressed breast phantoms for medical physics applications. Proc IWBI; 2020:1151304.
30. Lagarias JC, Reeds JA, Wright MH, Wright PE. Convergence properties of the Nelder-Mead simplex method in low dimensions. *SIAM J Optim*. 1998;9(1):112-147.

31. Fedon C, Caballo M, Longo R, Trianni A, Sechopoulos I. Internal breast dosimetry in mammography: experimental methods and Monte Carlo validation with a monoenergetic x-ray beam. *Med Phys*. 2018;45(4):1724-1737.
32. Fedon C, Caballo M, Sechopoulos I. Internal breast dosimetry in mammography: Monte Carlo validation in homogeneous and anthropomorphic breast phantoms with a clinical mammography system. *Med Phys*. 2018;45(8):3950-3961.
33. International Commission on Radiation Units and Measurements. *Tissue Substitutes in Radiation Dosimetry and Measurement International Commission on Radiation Units and Measurements*. Intl Commission on Radiation; 1989.
34. Hernandez AM, Boone JM. Tungsten anode spectral model using interpolating cubic splines: unfiltered x-ray spectra from 20 kV to 640 kV. *Med Phys*. 2014;41:042101.
35. Sempau J, Sánchez-Reyes A, Salvat F, Tahar HOB, Jiang SB, Fernández-Varea JM. Monte Carlo simulation of electron beams from an accelerator head using PENELOPE. *Phys Med Biol*. 2001;46:1163-1186. doi:10.1088/0031-9155/46/4/318
36. Cullen D, Hubbell JH, Kissel L. EPDL97: the evaluated photon data library, '97 version UCRL. *UCRL-50400*. 1997;6(5):50400.
37. Arce P, Bolst D, Bordage M-C, et al. Report on G4-Med, a Geant4 benchmarking system for medical physics applications developed by the Geant4 Medical Simulation Benchmarking Group. *Med Phys*. 2020;48(1):19-56.
38. Fedon C, Rabin C, Caballo M, et al. Monte Carlo study on optimal breast voxel resolution for dosimetry estimates in digital breast tomosynthesis. *Phys Med Biol*. 2018;64(1):015003.

How to cite this article: Caballo M, Rabin C, Fedon C, et al. Patient-derived heterogeneous breast phantoms for advanced dosimetry in mammography and tomosynthesis. *Med Phys*. 2022;49:5423–5438.
https://doi.org/10.1002/mp.15785